Measured close lightning leader-step electric field–derivative waveforms

J. Howard,[1,2] M. A. Uman,[1] C. Biagi,[1] D. Hill,[1] V. A. Rakov,[1] and D. M. Jordan[1]

Received 26 October 2010; revised 23 December 2010; accepted 4 January 2011; published 16 April 2011.

[1] We characterize the measured electric field–derivative (dE/dt) waveforms of lightning stepped-leader steps from three negative lightning flashes at distances of tens to hundreds of meters. Electromagnetic signatures of leader steps at such close distances have rarely been documented in previous literature. Individual leader-step three-dimensional locations are determined by a dE/dt TOA system. The leader-step field derivative is typically a bipolar pulse with a sharp initial half-cycle of the same polarity as that of the return stroke, followed by an opposite polarity overshoot that decays relatively slowly to background level. This overshoot increases in amplitude relative to the initial peak and becomes dominant as range decreases. The initial peak is often preceded by a "slow front," similar to the slow front that precedes the fast transition to peak in first return stroke dE/dt and E waveforms. The overall step-field waveform duration is typically less than 1 μs. The mean initial peak of dE/dt, range-normalized to 100 km, is 7.4 V m^{-1} μs^{-1} (standard deviation (S.D.), 3.7 V m^{-1} μs^{-1}, N = 103), the mean half-peak width is 33.5 ns (S.D., 11.9 ns, N = 69), and the mean 10-to-90% risetime is 43.6 ns (S.D., 24.2 ns, N = 69). From modeling, we determine the properties of the leader step currents which produced two typical measured field derivatives, and we use one of these currents to calculate predicted leader step E and dE/dt as a function of source range and height, the results being in good agreement with our observations. The two modeled current waveforms had maximum rates of current rise-to-peak near 100 kA μs^{-1}, peak currents in the 5–7 kA range, current half-peak widths of about 300 ns, and charge transfers of ~3 mC. As part of the modeling, those currents were propagated upward at 1.5 × 10^8 m s^{-1}, with their amplitudes decaying exponentially with a decay height constant of 25 m.

Citation: Howard, J., M. A. Uman, C. Biagi, D. Hill, V. A. Rakov, and D. M. Jordan (2011), Measured close lightning leader-step electric field–derivative waveforms, *J. Geophys. Res.*, *116*, D08201, doi:10.1029/2010JD015249.

1. Introduction

[2] *Howard et al.* [2010] employed an array of eight electric field–derivative (dE/dt) sensors separated by distances on the order of 100 m and configured in a time-of-arrival network to obtain 3-D source locations of (1) nearby lightning stepped-leader step pulses from a height of a few hundred meters above ground to near ground, (2) "leader burst" pulses following the step pulses and occurring beneath the step locations, (3) pulses occurring during the electric field "slow front" after the leader burst and associated with the ground attachment process and/or the beginning of the return stroke, and (4) the fast-transition dE/dt pulses associated with the return stroke radiation electric field transition to its initial peak. The 3-D location determined for stepped leader dE/dt pulses in three close stepped leaders by *Howard et al.* [2010] allows a full characterization of the close leader step waveform as a function of distance. A number of measurements of the salient characteristics of the electric field and electric field derivative of stepped leaders have been previously published for lightning at distances of tens of kilometers over saltwater [e.g., *Krider et al.*, 1977, 1992; *Weidman and Krider*, 1980; *Willett and Krider*, 2000; *Murray et al.*, 2005], and at closer distances over land [e.g., *Krider and Radda*, 1975; *Beasley et al.*, 1983; *Jerauld et al.*, 2008; *Howard et al.*, 2010], but there has been no detailed study of the field waveshape versus distance in the tens to hundreds of meters range. Here we present that characterization along with modeling of the leader step current, as a function of time and height, responsible for the stepped-leader electric field and electric field–derivative waveforms observed at ground level.

2. Experiment

[3] The data were acquired during summer 2006 and 2007 at the International Center for Lightning Research and Testing (ICLRT), a facility which occupies approximately 1 km^2 at the Camp Blanding Army National Guard Base in north-central Florida. The layout of the electric field–derivative time-of-arrival (TOA) network during the 2007 season is

[1]Department of Electrical and Computer Engineering, University of Florida, Gainesville, Florida, USA.
[2]Now at Sandia National Laboratories, Albuquerque, New Mexico, USA.

Copyright 2011 by the American Geophysical Union.
0148-0227/11/2010JD015249

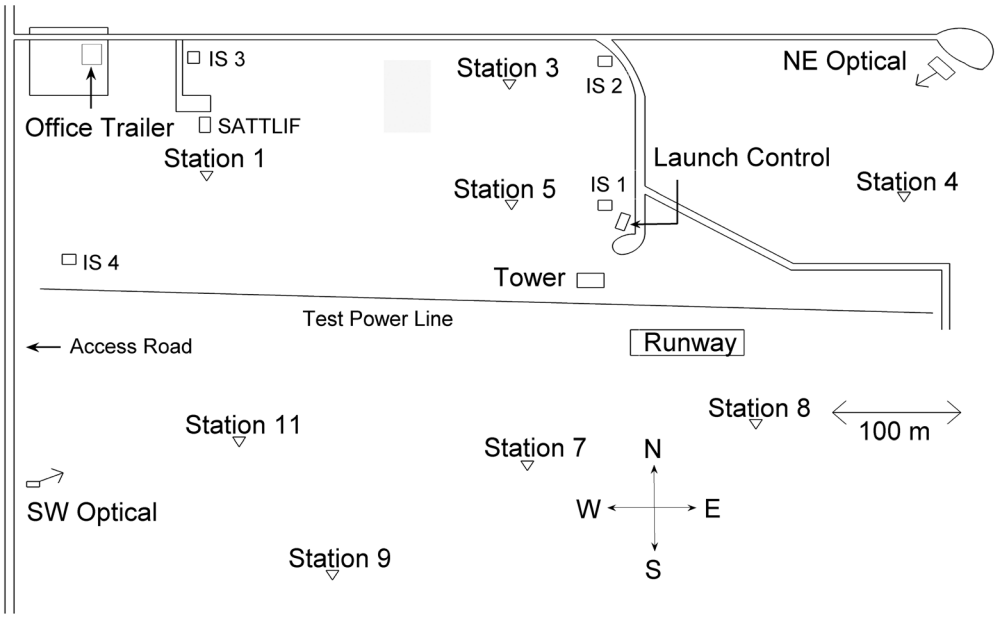

Figure 1. The TOA network at the ICLRT in 2007. Each station is denoted by a triangle and is labeled with its name.

shown in Figure 1. All dE/dt signals were transmitted from the sensing antennas to a central site via Opticomm MMV-120C fiber-optic links. At the central site the waveforms were filtered, digitized, and stored. The eight antennas in the TOA network were wideband (DC to 20 MHz, −3 dB) flat plate antennas, as also described by *Jerauld et al.* [2008]. The locations of the dE/dt sensors were accurately determined using an Electronic Total Station Traverse and a surveyor level. The signal transit-time delay for each sensor was measured end-to-end with an accuracy of ~2 ns. The dE/dt waveforms were recorded on five LeCroy four-channel digital storage oscilloscopes that sampled at 250 MHz for 2 ms with 1 ms of pretrigger, with the fifth oscilloscope redundantly recording one channel from each of the first four oscilloscopes in order to precisely synchronize all the time bases. More detailed information on the dE/dt sensors and the TOA network is given by *Howard et al.* [2010].

[4] *Howard et al.* [2010] describe the TOA location process and the associated location uncertainties. The process begins with the cross correlation of signals from pairs of individual channels to identify common events across multiple channels. Arrival times are then determined for the dominant initial peak of each dE/dt event. The set of arrival times selected for an event must all occur within a narrow window of time which is physically constrained by propagation paths and the transit time delays. Using this set of times, all combinations for $N \geq 5$ stations are used in a nonlinear least squares Marquardt algorithm, similar to that of *Thomas et al.* [2004] and *Koshak et al.* [2004], to determine the location and time of occurrence for the source. The solution is selected on the basis of a metric of the smallest product of the reduced Chi-square value and location uncertainty of the solution. The location uncertainties (errors) used in this metric are predicted from the covariance matrix returned by the solution algorithm. These location errors vary from one source to another and are dependent on the source location and the combination (geometry) of the stations utilized in the solution. The location uncertainties for the optimum solutions were often within 2–3 m in the horizontal directions and within 10 m in altitude for sources more than 50 m above ground.

3. Data and Analysis

[5] The data examined here were obtained from the stepped leaders of three downward-negative natural lightning flashes. MSE0604 was obtained on 2 June 2006 at approximately 2209 (UT); MSE0703 was obtained on 14 July 2007 at approximately 1625 (UT); and MSE0704 was obtained on 16 July 2007 at approximately 2327 (UT). All flashes occurred on or very near our research site, such that our TOA network could locate individual leader steps of the descending stepped leaders.

[6] The measured dE/dt waveform shown in Figure 2 (reproduced from *Howard et al.* [2010]) has a 16 μs duration near the time of the return stroke and contains two clear stepped-leader step (LS) waveforms (J and K) and other types of pulses, as noted in the Figure 2 caption. In general, dE/dt leader-step waveforms exhibit a variety of pulse shapes and features, often resulting from associated secondary pulses that are indicative of a complex and unique breakdown process within each step [*Howard et al.*, 2010], as observed for pulse J in Figure 2. Nevertheless, it is evident that there is a characteristic dE/dt leader-step waveform at close range. A decent illustration of this characteristic shape is given by pulse K in Figure 2 at −5 μs, as well as the same waveform on an expanded scale in Figure 3 at 2 μs. This characteristic shape is described as a bipolar pulse having a sharp initial peak with the same polarity as the return-stroke dE/dt pulse (Figure 2), followed by an opposite polarity overshoot which decays relatively slowly to background level. As we shall discuss, the magnitude of the overshoot generally increases

21562202d, 2011, D8, Downloaded from https://agupubs.onlinelibrary.wiley.com/doi/10.1029/2010JD015249, Wiley Online Library on [28/07/2025]. See the Terms and Conditions (https://onlinelibrary.wiley.com/terms-and-conditions) on Wiley Online Library for rules of use; OA articles are governed by the applicable Creative Commons License

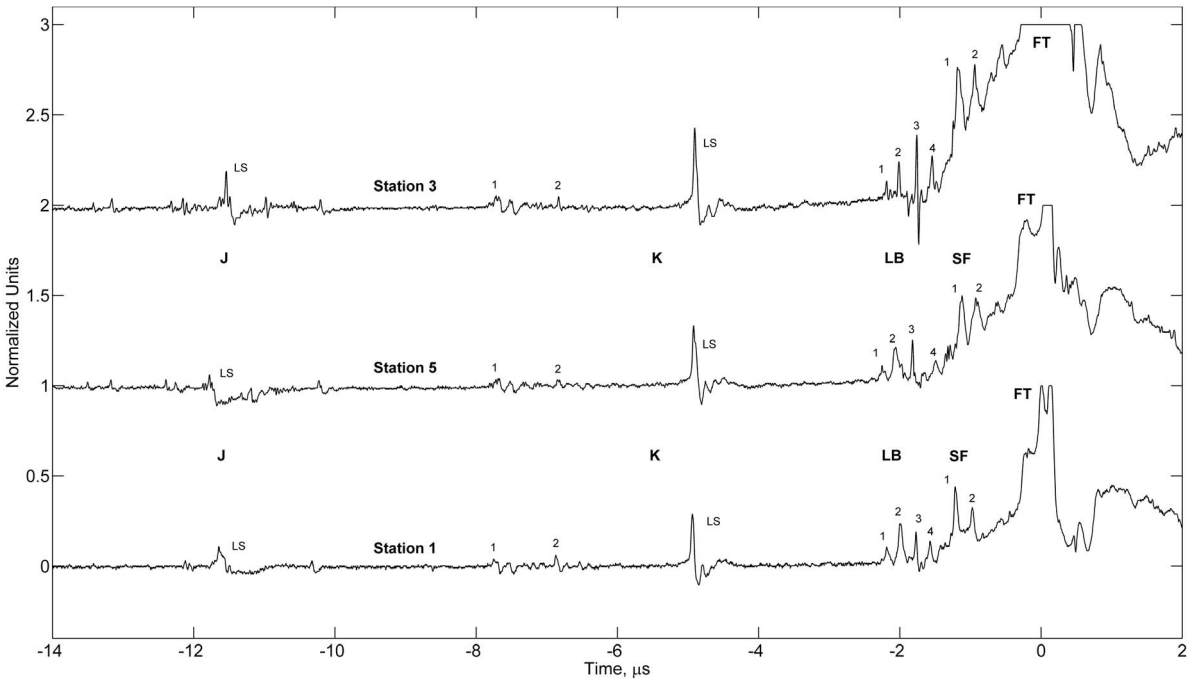

Figure 2. The dE/dt waveforms from the three stations closest to the first stroke of MSE0604 on a 16 μs scale. LS identifies leader step pulses, LB is leader burst pulses, SF is slow front pulses, and FT is the fast transition pulse.

with decreasing distance to the dE/dt source. The initial peak is often preceded by a "slow front," similar to the slow front that precedes the fast transition to peak in first return stroke dE/dt and E.

[7] In addition to illustrating the characteristic leader pulse shape, Figure 3 shows the template that will be used to present additional leader-step dE/dt waveforms. Figures 3, 5, 6, 7, 8, and 9 include either four or five separate waveforms from

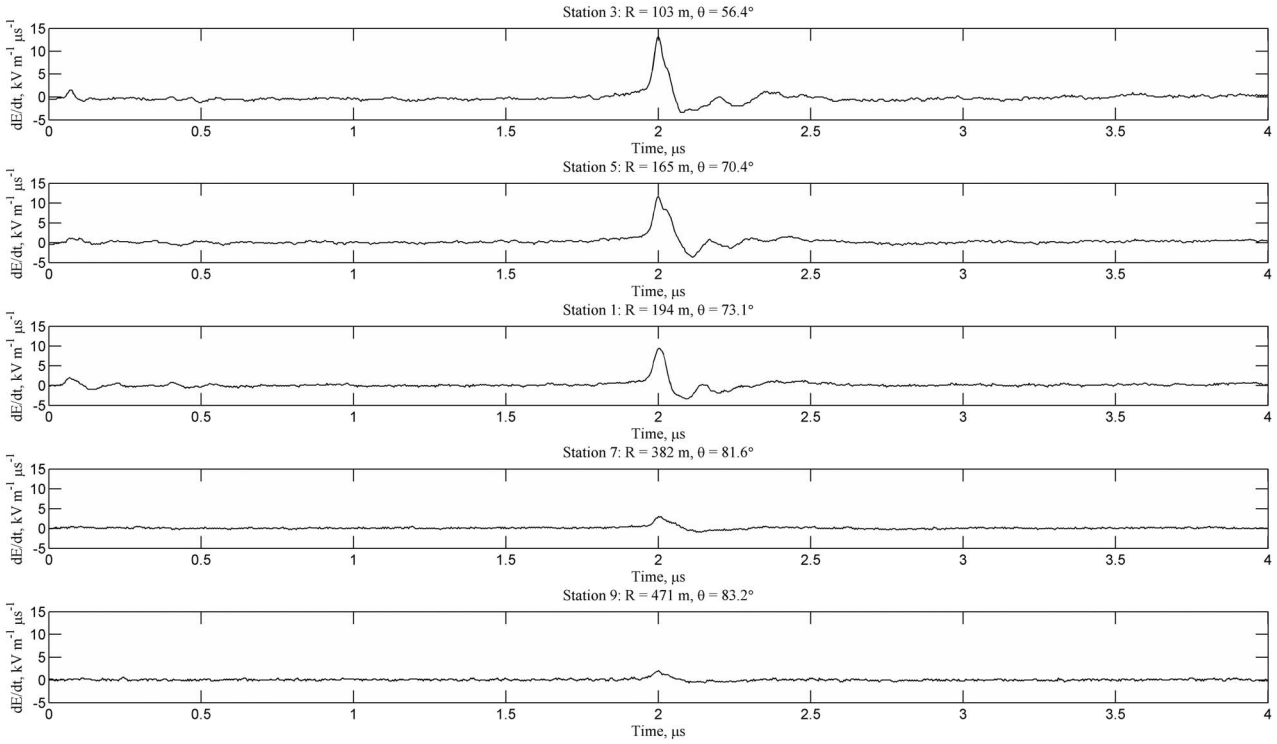

Figure 3. A leader-step dE/dt at five stations from the lightning record shown for three stations in Figure 2. The leader step occurs at 2 μs in these plots but at −5 μs in Figure 2.

21562202d, 2011, D8, Downloaded from https://agupubs.onlinelibrary.wiley.com/doi/10.1029/2010JD015249, Wiley Online Library on [28/07/2025]. See the Terms and Conditions (https://onlinelibrary.wiley.com/terms-and-conditions) on Wiley Online Library for rules of use; OA articles are governed by the applicable Creative Commons License

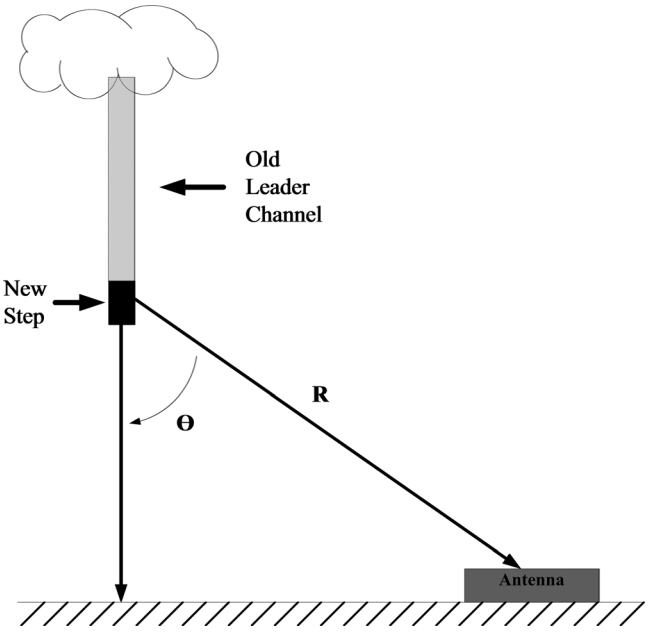

Figure 4. Diagram illustrating the spatial relationship between the leader step and the antenna.

different receiving stations, with all waveforms in a single figure displayed on the same time and amplitude scales. Each waveform is labeled with its corresponding station number, the length of the distance vector $\boldsymbol{R}$ pointing from the leader step to the dE/dt antenna, and the angle (θ) between the vector $\boldsymbol{R}$ and the downward vertical, as illustrated in Figure 4. The waveforms in Figures 3, 5, 6, 7, 8, and 9 are shown with increasing $|\boldsymbol{R}|$ from top to bottom. As shown in Figure 4, the leader-step channel is assumed to be vertical, an assumption which may not always be valid.

[8] A step dE/dt pulse from lightning event MSE0703 that exhibits the characteristic leader-step waveshape, similar to that of pulse K from MSE0604 in Figure 3, is shown in Figure 5. Figures 6 and 7 illustrate leader steps in which the shape of the leader-step pulse is affected at one or more sensors by their distance and orientation relative to the step. In Figure 6, the initial sharp peak of the leader pulse is essentially absent from the closest waveform observed at Station 3. The same is true for both the Station 3 and Station 5 waveforms in Figure 7, although they are the two closest stations to the step. As will be discussed in section 4, the electromagnetic radiation from an assumed vertical, finite-length current-carrying element (used to approximate the leader-step channel) is dependent on the current distribution in the element and the position (range and angle) of the element relative to the observer. Further, there are three components (electrostatic, induction, and radiation) comprising the observed electric field (or electric field derivative). The radiation component is the only component that approaches zero as the assumed-vertical current-carrying element (Figure 4) approaches a position directly above the observation point, that is, when the angle (θ) in Figure 4 approaches zero; or, what is equivalent for a nonvertical step, when the step is along the observer's line-of-sight from the antenna. Nevertheless, the initial peak of leader-step dE/dt pulses is generally dominated by the radiation component, since radiation fields, as we shall see, are the dominant initial field component for ranges beyond 100 m or so, and the stepped leader

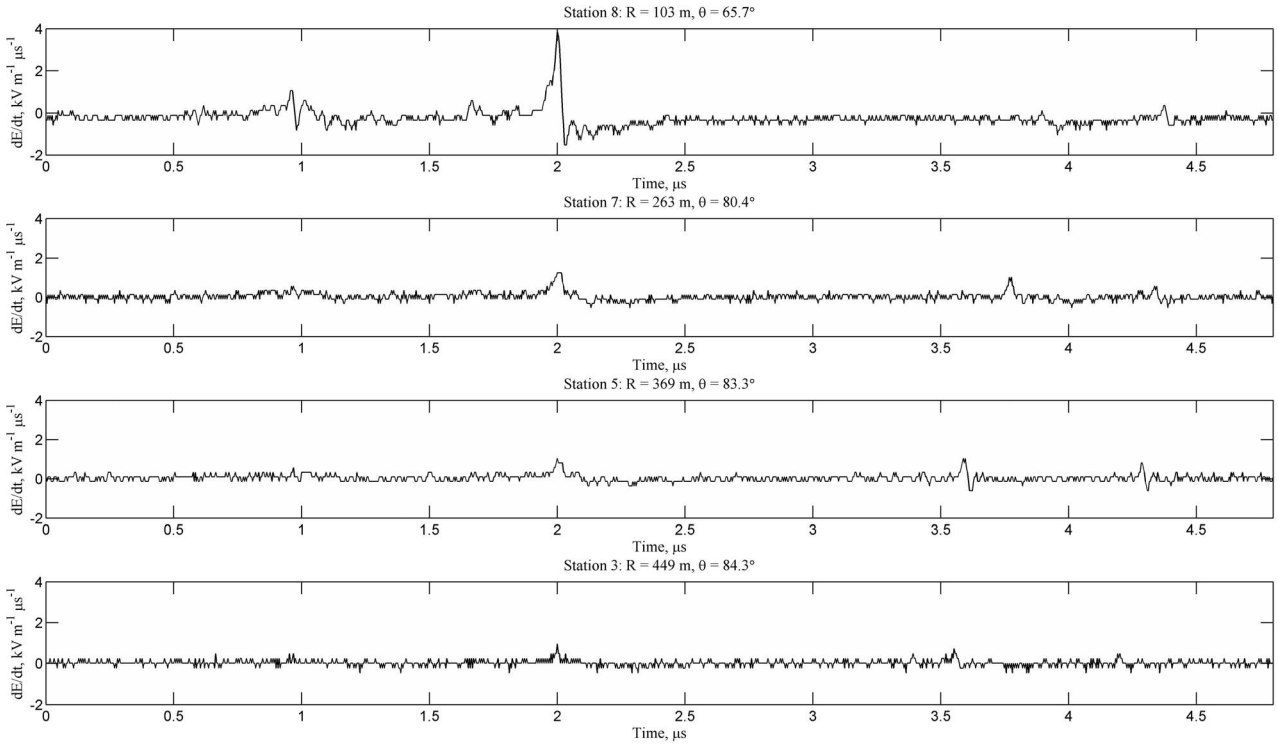

Figure 5. A leader-step dE/dt from lightning event MSE0703 exhibiting the characteristic pulse shape. The leader step occurs at 2 μs.

21562202d, 2011, D8, Downloaded from https://agupubs.onlinelibrary.wiley.com/doi/10.1029/2010JD015249, Wiley Online Library on [28/07/2025]. See the Terms and Conditions (https://onlinelibrary.wiley.com/terms-and-conditions) on Wiley Online Library for rules of use; OA articles are governed by the applicable Creative Commons License

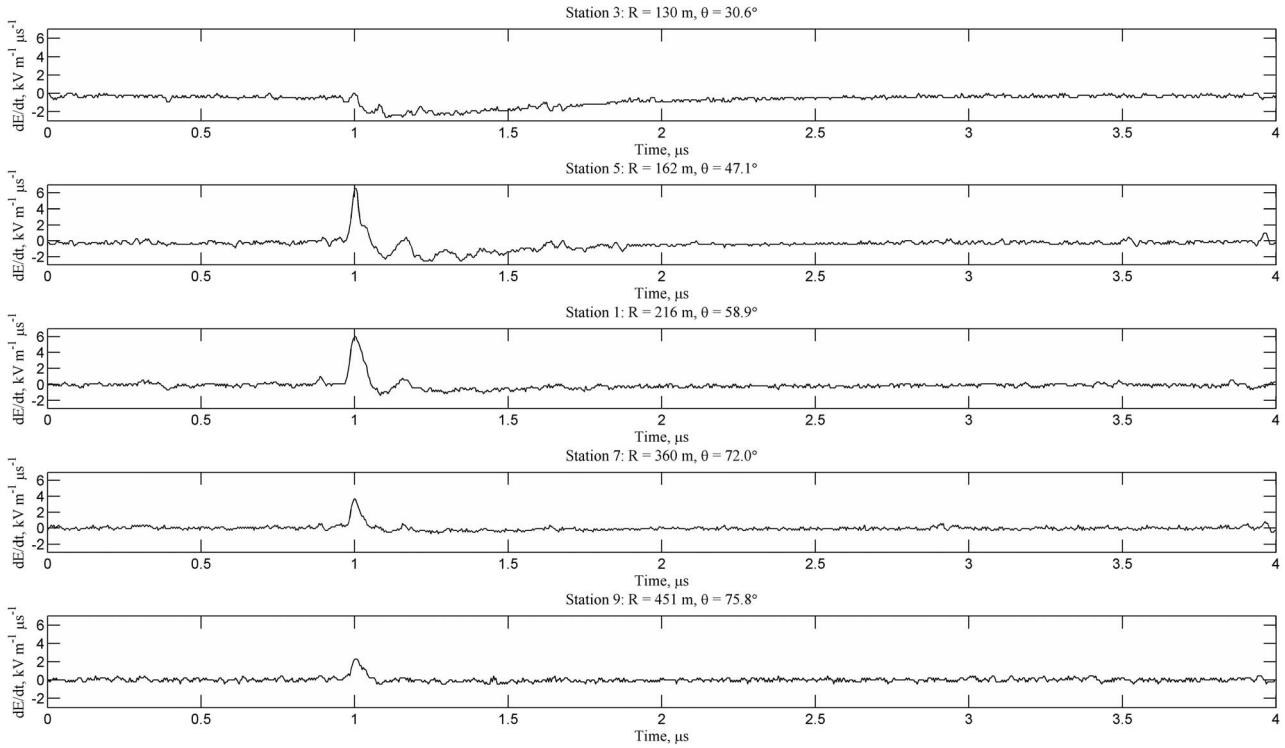

Figure 6. A leader-step dE/dt from MSE0604 in which the closest station is missing the initial peak. The step field occurs at 1 μs.

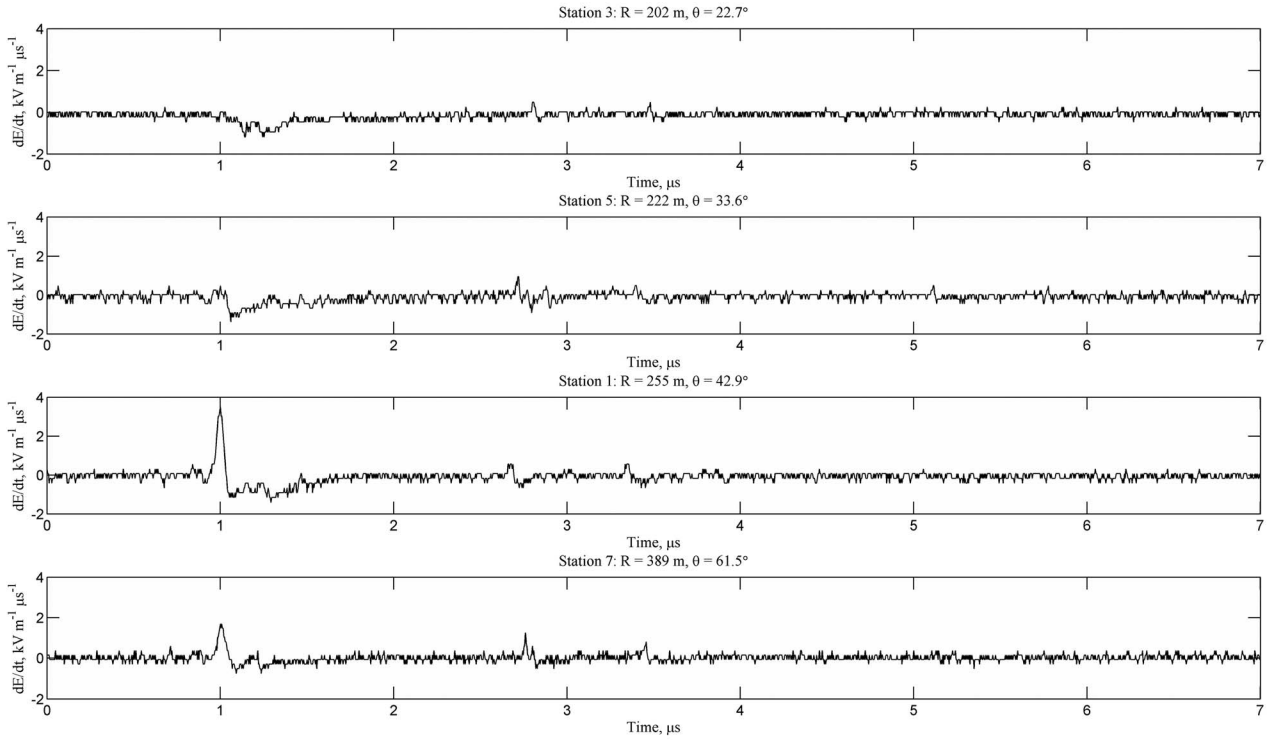

Figure 7. A leader-step dE/dt from MSE0604 where the two closest stations are missing the initial peak. The step field occurs at 1 μs.

21562202d, 2011, D8, Downloaded from https://agupubs.onlinelibrary.wiley.com/doi/10.1029/2010JD015249, Wiley Online Library on [28/07/2025]. See the Terms and Conditions (https://onlinelibrary.wiley.com/terms-and-conditions) on Wiley Online Library for rules of use; OA articles are governed by the applicable Creative Commons License

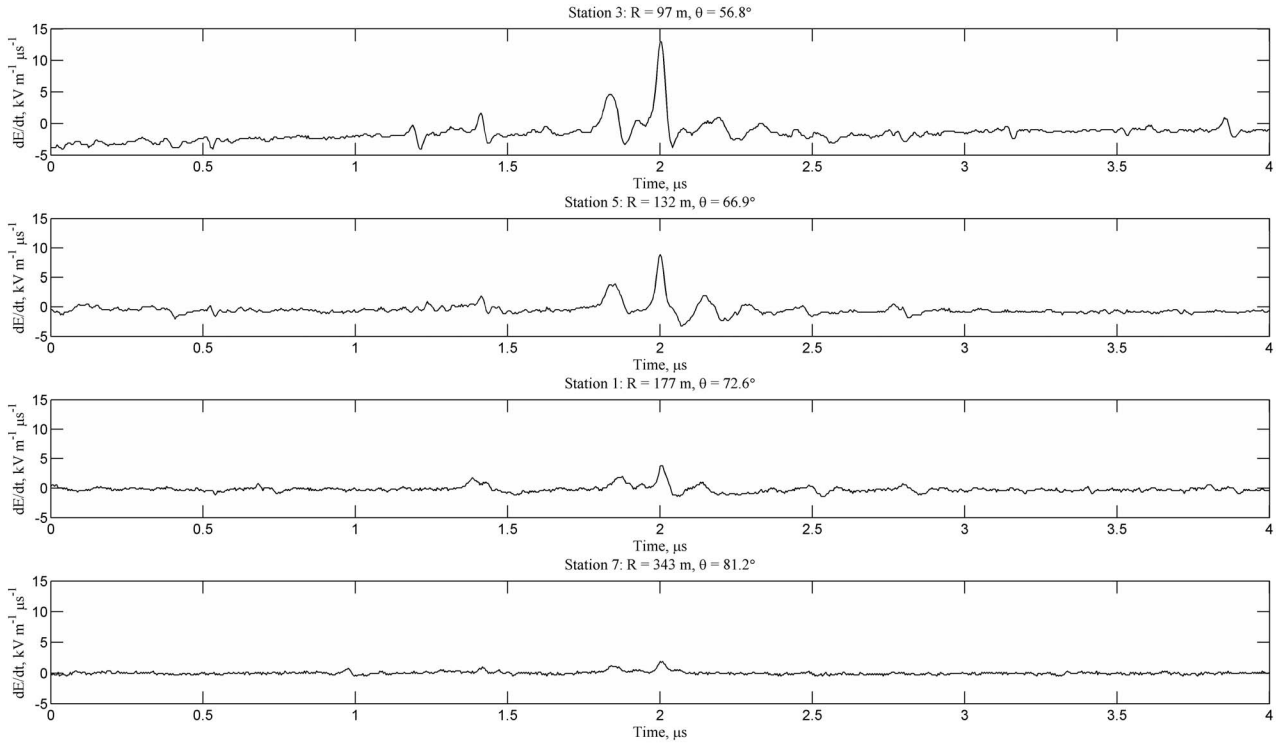

Figure 8. A leader-step dE/dt from MSE0604 with secondary pulses. The primary step occurs at 2 μs.

channel is rarely overhead or exactly along the line of sight. As we shall also discuss, the close electrostatic field is of the opposite polarity to the initial radiation peak and increases in magnitude with decreasing range.

[9] Figures 8 and 9 provide examples of leader-step waveforms that contain secondary pulses superimposed on and near the characteristic pulse shape. These are the pulses designated secondary pulses by *Howard et al.* [2010], who divided them into (1) the before-step (BS) and (2) the after-step (AS) pulses. Sometimes the BS secondary pulses occur with such temporal proximity to the dominant peak that they cause significant distortion of the slow front, making it impossible to determine the slow front contribution. The leader step shown in Figure 3 exhibits a slow front that is not distorted by any BS secondary pulses.

4. Statistics

[10] Some of the TOA network dE/dt antennas are collocated with electric field (E) antennas. Integrating a dE/dt waveform from one of the TOA stations will reproduce the waveshape of the directly measured electric field at the same station with great accuracy; however, the resultant waveform is sometimes smaller in amplitude than the directly measured E-field waveform [*Howard et al.*, 2010; *Jerauld et al.*, 2008]. The scaling factor needed to correct for this unexplained discrepancy, which usually varies from about 1.2 to 2, is different at each station and changes from day to day. Interestingly, the scaling factor remains constant at each station for flashes that occur on the same day. It is unclear if the dE/dt, E-field, or both measurements are in error, but plotting electric field changes versus distance generally results in an inverse dependence with distance, while plotting peak dE/dt values versus distance does not always. Despite this reservation in dE/dt calibration, it is of value to determine the mean peak of the dE/dt leader-step waveforms (range normalized to 100 km using an inverse distance relationship) so as to be able to compare that quantity with the previous means determined for distant measurements over salt water. Propagation over salt water, a moderately good conductor, is thought to provide minimal waveform distortion.

[11] We obtain values for the leader pulse half-peak width, risetime, and peak value from the three natural flashes studied by *Howard et al.* [2010]. The half-peak values (T_{HPW}) of the dE/dt pulses are a measure of the fast-rising portion of the corresponding electric field pulses. As discussed above, leader steps that have a small angle (θ) with respect to vertical (see Figure 4) generally have a diminished initial peak. Hence, it would seem using leader steps which are relatively high above the site would produce much smaller peak values and potentially contaminate these calculations intended to compare with data from distant leaders which are nearly level with the observer. Therefore, this analysis only includes leader steps that occurred within 100 μs of the return stroke, i.e., only leader steps occurring near the ground. Further, for measuring the peak values of the steps, only dE/dt pulses that registered an initial peak of 1 kV m^{-1} μs^{-1} or greater were used, to ensure adequate amplitude resolution (sufficiently larger than system background noise). Finally, pulses that exhibited any significant baseline offset or secondary pulses immediately prior to the start of the main leader pulse were excluded from the data set. With these criteria, 103 waveforms produced by 21 different leader steps were analyzed in the three flashes considered. Each leader step was observed

21562202d, 2011, D8, Downloaded from https://agupubs.onlinelibrary.wiley.com/doi/10.1029/2010JD015249, Wiley Online Library on [28/07/2025]. See the Terms and Conditions (https://onlinelibrary.wiley.com/terms-and-conditions) on Wiley Online Library for rules of use; OA articles are governed by the applicable Creative Commons License

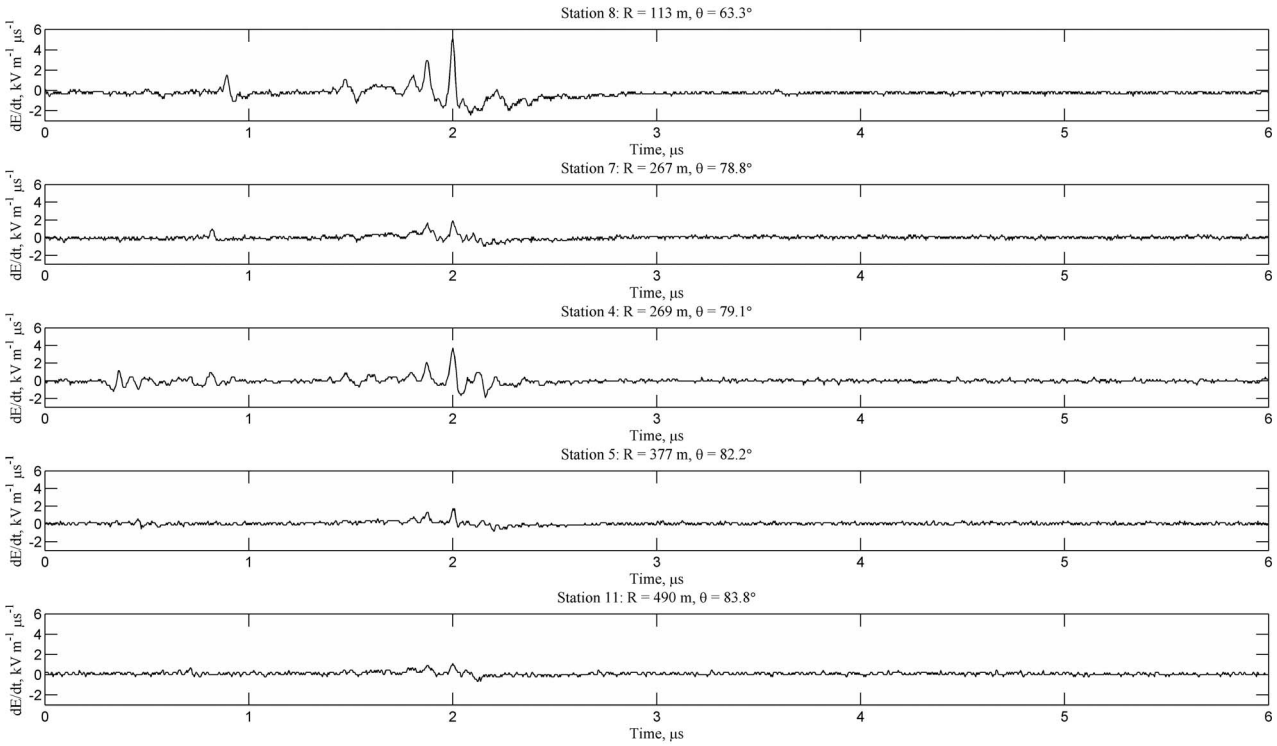

Figure 9. A leader step from MSE0703 with secondary pulses. The primary step occurs at 2 μs.

with at an average of 5 stations. The histogram for these peak dE/dt values normalized to 100 km, with no account taken of their angle with respect to the vertical, is shown in Figure 10. The mean peak of the dE/dt range-normalized step pulses was found to be 7.4 V m^{-1} μs^{-1}, with a standard deviation of 3.7 V m^{-1} μs^{-1}. *Krider et al.* [1992] give a measured mean value of 13 V m^{-1} μs^{-1} for 17 events. Recall that our measurements may be underestimated by a factor of 1.2 to 2 because of system calibration and are also reduced from the maximum possible due to the line of sight being nonperpendicular to the step.

[12] The half-peak width and 10–90% risetime of the leader steps were measured for dE/dt pulses exceeding 1.5 kV m^{-1} μs^{-1}, again to ensure proper amplitude resolution. This criterion reduces the previous data set of 103 waveforms to 69 waveforms produced by 20 different leader steps in three flashes. The normal sampling time interval of the measured data (4 ns) did not permit a precise calculation

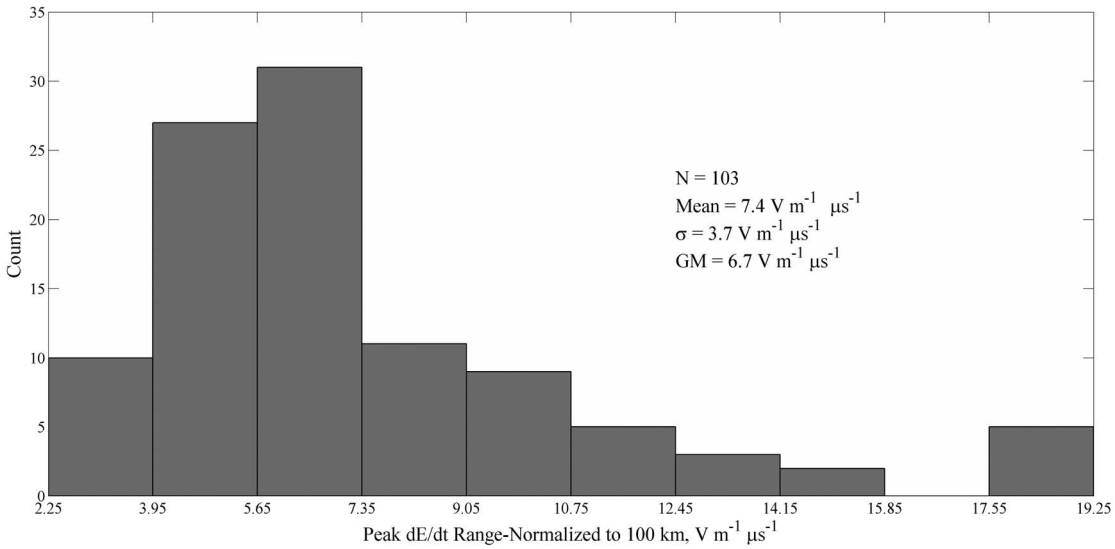

Figure 10. Histogram of peak dE/dt range-normalized to 100 km. The sample size (N), mean, standard deviation (σ), and geometric mean (GM) are specified in the plot.

21562202d, 2011, D8, Downloaded from https://agupubs.onlinelibrary.wiley.com/doi/10.1029/2010JD015249, Wiley Online Library on [28/07/2025]. See the Terms and Conditions (https://onlinelibrary.wiley.com/terms-and-conditions) on Wiley Online Library for rules of use; OA articles are governed by the applicable Creative Commons License

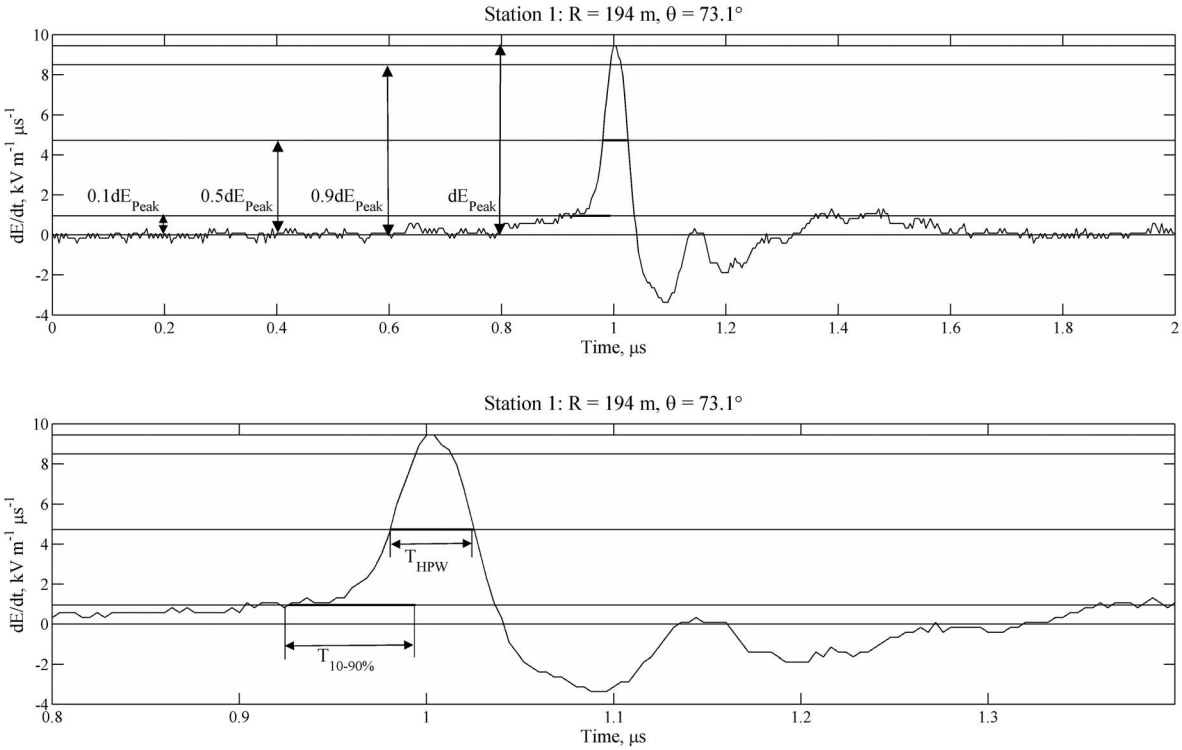

Figure 11. Illustration of measurements of the half-peak width and 10–90% risetime.

of the half peak or 10–90% risetime, so linear interpolation was used to improve the sample resolution to 0.25 ns. After interpolation, we selected the peak value, 0.9 peak value, 0.5 peak value, and the 0.1 peak value. A computer routine was used to identify all points with amplitude equal to or greater than the 0.5 peak value, and then the routine found the time difference between the first and last points. Similarly, the routine identified the sample points lying between the 0.1 peak and 0.9 peak values on the rising edge and found the time difference between the first and last samples. An illustration of how these values were measured is found in Figure 11.

[13] After these values were obtained, both the half-peak widths and the 10–90% risetimes were each plotted versus distance (R) to make sure there was no obvious distance dependence over the range we observed. There was none. Finally, to determine if the half-peak width was dependent on the pulse peak amplitude, we plotted the half-peak widths versus peak dE/dt normalized to 100 km. No significant correlation was observed. Since there does not appear to be any bias with distance or peak amplitude, we can analyze the distributions for the half-peak widths and 10–90% risetimes. The half-peak width distribution is shown in Figure 12 and the 10–90% risetime distribution is shown in Figure 13. The means, standard deviations, and geometric means for these distributions are shown in Figures 12 and 13. Our mean 10–90% risetime for the leader-step dE/dt pulses is 43.6 ns (standard deviation of 24.2 ns) and our mean half-peak width is 33.5 ns (standard deviation of 11.9 ns). The latter value can be compared with the value determined from the dE/dt measurements with field propagation over salt water of *Willett and Krider* [2000] who found a mean half-peak width of 54 ns (standard deviation of 17 ns). No 10–90% risetime values for leader-step electric field–derivative waveforms are apparently found in the literature.

5. Modeling

[14] We model the leader step channel as a finite-length vertical antenna which is composed of a number of small dipoles [e.g., *Uman and McLain*, 1969; *Uman et al.*, 1975; *Thottappillil et al.*, 1997]. Maxwell's equations can be used to calculate the electric and magnetic field contributions from each infinitesimal dipole if the dipole current is assumed, and the total electric and magnetic fields produced by the antenna can be determined by spatial integration over the component dipoles comprising the antenna. The geometry of this problem, which is most easily represented in cylindrical coordinates, is illustrated in Figure 14. Following some slight manipulation of the solutions presented by *Uman et al.* [1975], including a generalization for a channel that begins at any altitude, the vertical electric field and horizontal magnetic field can be expressed as

$$E_z(r,t) = \frac{1}{2\pi\varepsilon_0}\left[\int_{H_B}^{H_T}\frac{2z'^2-r^2}{R^5}\int_{R/c}^{t} i(z',\tau-R/c)\,d\tau\,dz' + \int_{H_B}^{H_T}\frac{2z'^2-r^2}{cR^4}\cdot i(z',t-R/c)\,dz' - \int_{H_B}^{H_T}\frac{r^2}{c^2R^3}\frac{\partial i(z',t-R/c)}{\partial t}\,dz'\right] \quad (1)$$

$$\mathrm{B}_\phi(r,t) = \frac{\mu_o}{2\pi}\left[\int_{H_B}^{H_T}\frac{r}{R^3}i(z',t-R/c)\,dz' + \int_{H_B}^{H_T}\frac{r}{cR^2}\frac{\partial i(z',t-R/c)}{\partial t}\,dz'\right]. \quad (2)$$

21562202d, 2011, D8, Downloaded from https://agupubs.onlinelibrary.wiley.com/doi/10.1029/2010JD015249, Wiley Online Library on [28/07/2025]. See the Terms and Conditions (https://onlinelibrary.wiley.com/terms-and-conditions) on Wiley Online Library for rules of use; OA articles are governed by the applicable Creative Commons License

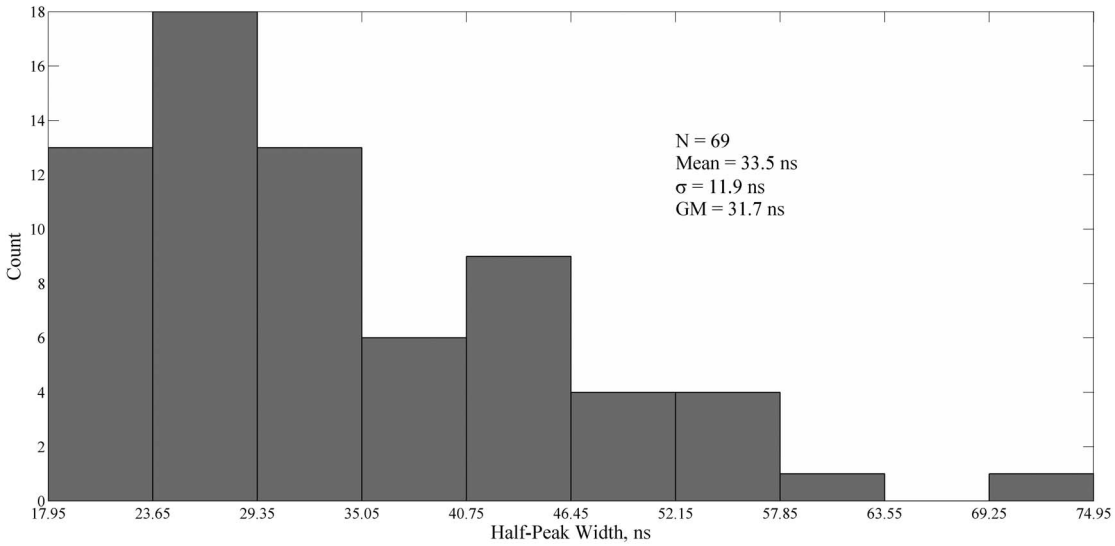

Figure 12. Histogram of half-peak width of dE/dt leader pulses. The sample size (N), mean, standard deviation (σ), and geometric mean (GM) are specified in the plot.

The quantities H_B and H_T are the heights of the bottom and top of the channel, respectively. The primed coordinates indicate a source point while unprimed coordinates indicate the field (observation) point. At height z' a current $i(z', t)$ flows in a infinitesimal dipole of length dz'. R is the distance between the source channel section dz' at height z' and the observation point at horizontal distance r. Hence, $\boldsymbol{R} = \boldsymbol{r} - \mathbf{z}'$ and $R = R(z') = \sqrt{(z'^2 + r^2)}$.

[15] The three terms of equation (1) are referred to as the "electrostatic" (related to the integral of the current, or the charge transferred), "induction" (related to the current), and "radiation" (related to the current derivative) components, each with a different dependence on distance. The electrostatic component has the strongest distance dependence and is the only component that is nonzero after the current ceases to flow. The radiation component has the weakest distance dependence and becomes the dominant field component as distance increases. Similarly, the two magnetic field terms in equation (2) are the induction and radiation components. Since there is no term that is related to the integral of the current, the magnetic field is always zero when no current is flowing.

[16] While equations (1) and (2) provide the means of calculating electric and magnetic fields from a given current distribution, they do not provide the current distribution itself. Since current cannot be measured directly at any elevated point in the lightning channel, the current distribution must be assumed from some reasonable model. For return strokes, which are probably the most modeled lightning process, there are several types of models. The simplest group of these models, dubbed "engineering" models by *Rakov and Uman* [1998], simply provide an equation relating the longitudinal

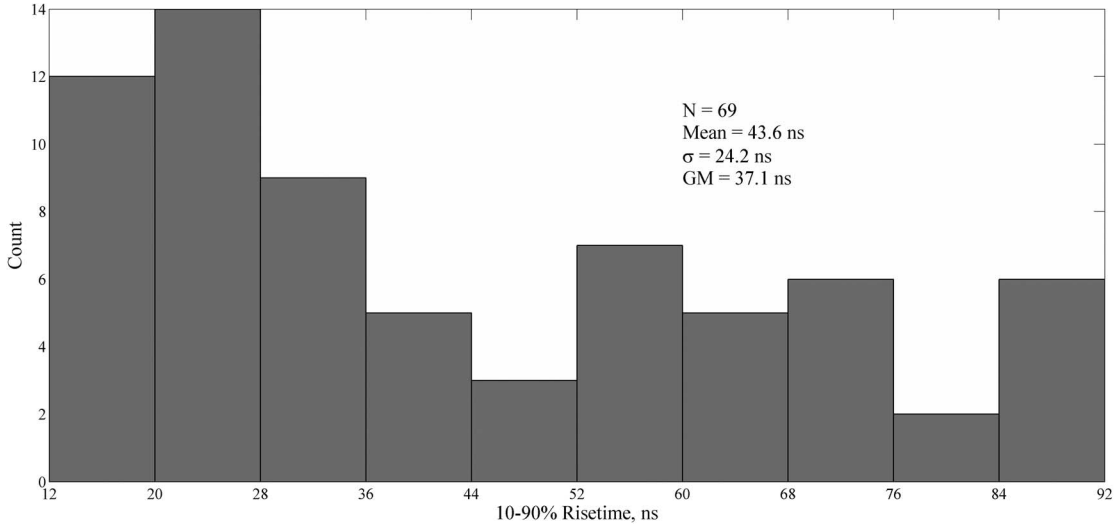

Figure 13. Histogram of 10–90% risetime for dE/dt leader pulses. The sample size (N), mean, standard deviation (σ), and geometric mean (GM) are specified in the plot.

21562202d, 2011, D8, Downloaded from https://agupubs.onlinelibrary.wiley.com/doi/10.1029/2010JD015249, Wiley Online Library on [28/07/2025]. See the Terms and Conditions (https://onlinelibrary.wiley.com/terms-and-conditions) on Wiley Online Library for rules of use; OA articles are governed by the applicable Creative Commons License

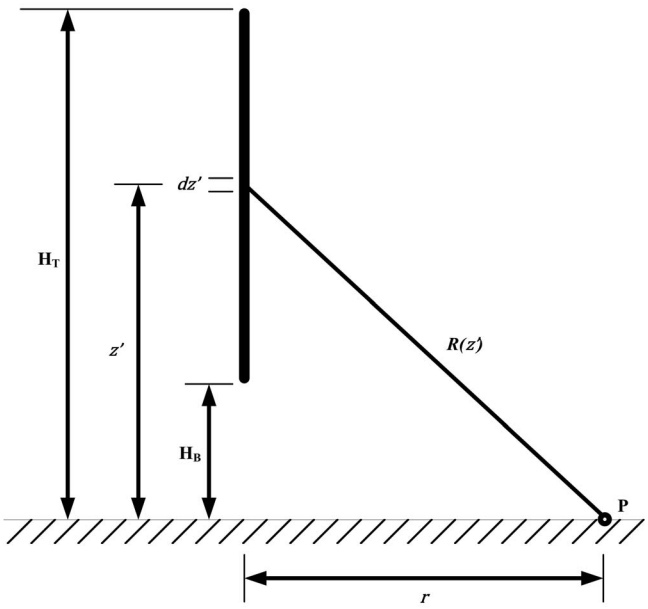

Figure 14. Illustration of geometry involved in calculating electric and magnetic fields on ground at horizontal distance r from a straight and vertical antenna of length $H = H_T - H_B$ over a perfectly conducting ground plane.

channel current $i(z', t)$ at any height z' and any time t to the current $i(0,t)$ at the channel origin, $z' = 0$.

[17] The transmission line (TL) model [*Uman and McLain*, 1969] is a popular "engineering" return-stroke model [*Willett et al.*, 1988; *Schoene et al.*, 2003] that assumes the current waveform starts at the bottom of the channel (typically at ground, $H_B = 0$) and propagates upward at constant velocity v with no attenuation or distortion. This is described mathematically as equation (3).

$$i(z', t) = i\left(H_B, t - z'/v\right). \tag{3}$$

The TL model can be easily adapted to include a linear [*Rakov and Dulzon*, 1987] and exponential [*Nucci et al.*, 1988] current amplitude decay with height, represented by equations (4) and (5), respectively.

$$i(z', t) = \left(1 - \frac{z' - H_B}{H}\right) \times \; i(0, t - z'/v) \tag{4}$$

$$i(z', t) = e^{-(z'-H_B)/\lambda} \times \; i(0, t - z'/v) \tag{5}$$

The goal here is to model leader steps. The field calculations (equations (1) and (2)), the TL model (equation (3)), and the current decay modifications (equations (4) and (5)) are easily adapted to a finite vertical channel located at an arbitrary height. We desire to model the electric field derivative and not the electric field itself. This can be accomplished by differentiating the calculated electric field or by differentiating the current-related term associated with each field component prior to calculating the field. There is no problem with performing such calculations as long as the current derivative (associated with the radiation component of equation (1)) is a differentiable function.

[18] Finally, we note that the presence of a finitely conducting ground results in the selective attenuation of the high-frequency components of the electric and magnetic fields radiated by the lightning discharge [e.g., *Uman et al.*, 1976; *Cooray*, 1987; *Cooray et al.*, 2000, *Cooray*, 2009]. This attenuation is generally referred to as "propagation effects." Propagation effects cause the peak value, risetime, and half-peak width of the lightning generated fields and field derivatives to deviate (peak values decrease, risetime and half-peak width increases) from their values that would be measured over a perfectly conducting ground. A quantification of propagation effects involves a modification to the field contribution from each of the infinitesimal dipoles to account for the finite ground conductivity [e.g., *Norton*, 1937; *Cooray*, 1987]. In the results that follow, no attempt was made to account for propagation effects, possibly causing the discrepancies observed between the peak values of the calculated and measured fields for some of the more distant cases.

[19] At this point, the expressions necessary for calculating the lightning fields (equations (1) and (2) and the engineering models necessary for describing the current distribution) have been introduced, but the current waveform itself has not yet been defined. A popular current waveform is the Heidler function [*Heidler*, 1985], which is expressed by equation (6).

$$I(t) = \frac{I_0}{\eta} \frac{(t/\tau_1)^n}{(t/\tau_1)^n + 1} e^{-t/\tau_2} \tag{6}$$

Jerauld [2007], who in his PhD dissertation presents a rare attempt at leader-step modeling, used the Heidler function to model one step from a dart-stepped leader in a rocket-triggered flash and one step from a natural stepped leader. For the dart-stepped leader step, *Jerauld* [2007] had electric and magnetic field derivative measurements located precisely 15 and 30 m from the strike object, and video images were used to estimate the height of the modeled leader step. *Jerauld* [2007] selected current propagation speeds, based on model agreement with the measured fields, of 1.5×10^8 m s^{-1} and 1.7×10^8 m s^{-1} for the rocket-triggered lightning step and natural lightning step, respectively. In both cases, the current was assumed to decay exponentially with height, with a decay constant of 22 m. We find that a single Heidler function current waveform cannot adequately reproduce those measured dE/dt waveforms that decrease or increase in value (exhibit slow fronts) just prior to the main step pulse, as in pulse K of Figure 2, and hence a current function with a slow-rising front is necessary to match many of the measured leader step waveforms.

[20] The current derivative expression, equation (7), that is used here and that produces dE/dt waveforms closely approximating the measure data was introduced by *Jerauld* [2007] for the purpose of modeling the current derivative of first strokes.

$$\frac{dI(t)}{dt} = \left(\frac{\alpha_1}{1 + \left(\frac{t - T_{peak}}{\gamma}\right)^2} + \frac{\alpha_2}{1 + \left(\frac{t - T_{peak}}{0.5T_{peak}}\right)^2}\right) \times \left(\frac{1 + \beta}{1 + e^{\left(t - T_{peak} - 3\gamma\right)/\gamma}} - \beta\right) \times \left(1 - \frac{1}{1 + e^{4\left(t - 0.5T_{peak}\right)/T_{peak}}}\right). \tag{7}$$

215622024, 2011, D8, Downloaded from https://agupubs.onlinelibrary.wiley.com/doi/10.1029/2010JD015249, Wiley Online Library on [28/07/2025]. See the Terms and Conditions (https://onlinelibrary.wiley.com/terms-and-conditions) on Wiley Online Library for rules of use; OA articles are governed by the applicable Creative Commons License

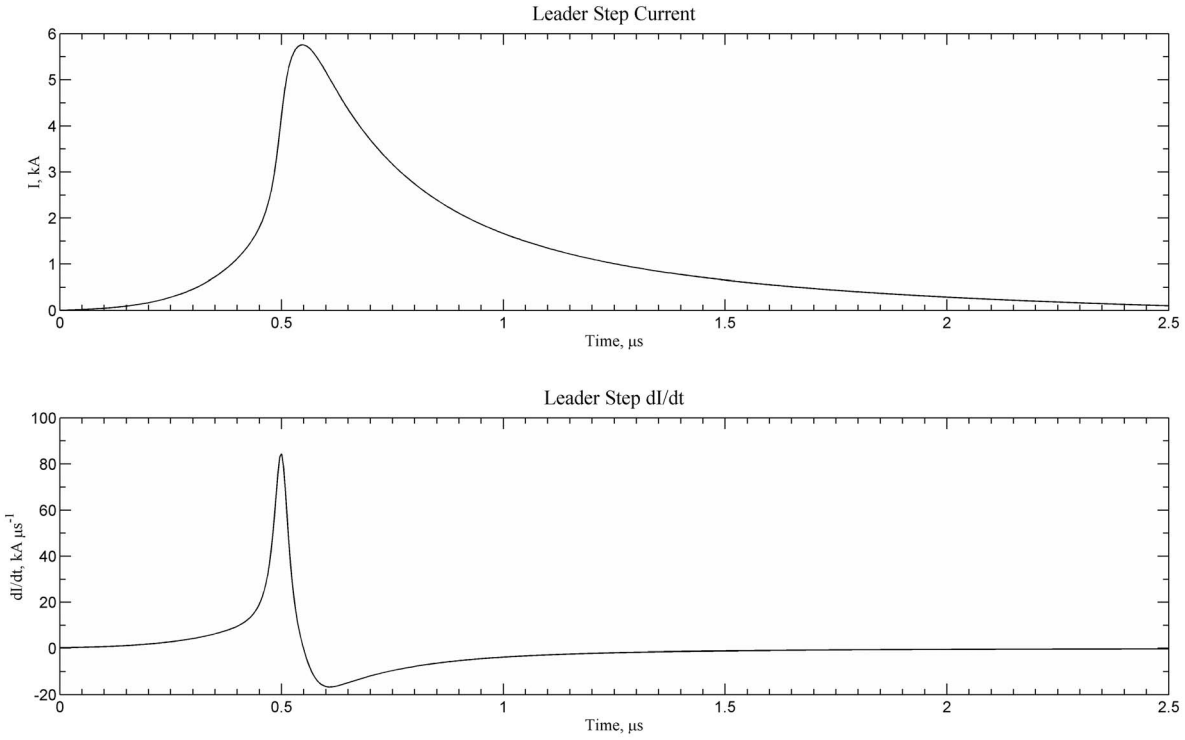

Figure 15. Current and current derivative waveforms used in the modeling of Step A. The current derivative waveform was generated using equation (7) with the parameters $T_{peak} = 0.5$ μs, $\alpha_1 = 100$ kA μs^{-1}, $\alpha_2 = 10$ kA μs^{-1}, $\beta = 1.73$, and $\gamma = 20$ ns.

The right-hand side of equation (7) is the product of three terms, having a total of 5 adjustable parameters. The first term in brackets is related to the general shape of the dI/dt waveform, including the slow front and fast transition to peak. The quantities α_1 and α_2 affect the maximum amplitudes of the fast transition and slow front, respectively. The quantity T_{peak} sets the time of the peak of the waveform, while γ is related to the width of the fast transition derivative pulse. The second term in brackets in equation (7) is related to the decay of the waveform after the peak, and is adjustable with the parameter β (a sensitive parameter which if too small causes the waveform to increase beyond zero and if too large causes the waveform to become increasingly negative). Finally, the third term assures that the slow front begins at a value at or very near zero. Equation (7) is complex and not very intuitive, but it does provide an adequate slow front followed by a fast transition that occurs very near the specified parameter T_{peak}. The current waveform itself can be obtained by numerically integrating the dI/dt waveform generated by equation (7).

[21] Figure 15 shows the current derivative and current used for example Step A with the parameters in equation (7) being given in the Figure 15 caption. The resultant current waveform has a peak value, half-peak width, and charge transfer of 5.8 kA, 300 ns, and 2.9 mC, respectively. The peak dI/dt value is about 84 kA μs^{-1}. Figure 16 shows the modeling results for Step A. It is of particular interest that the model predicts a negative dip in the dE/dt waveform just prior to the primary leader step in the Station 3 waveform, which agrees with the measured waveform. Note that a current model based on the single Heidler function is incapable of reproducing this feature. The assumed propagation velocity was 1.5×10^8 m s^{-1} and the assumed exponential current decay height constant was 25 m.

[22] The current derivative and current shown in Figure 17 are used as inputs to obtain the modeling results for Step B shown in Figure 18, with the parameters for equation (7) given in the Figure 17 caption. The current waveform has a peak value, half-peak width, and charge transfer of 6.5 kA, 290 ns, and 3 mC, respectively. The peak dI/dt value was about 98 kA μs^{-1}. The model uses the propagation velocity 1.5×10^8 m s^{-1} and the exponential current decay height constant of 25 m. Similar to the previous modeling example (Step A), an important feature in the modeled dE/dt leader-step waveform, the slow rise preceding the primary pulse in this case, is reproduced by our current model, but not with the single Heidler function.

[23] The current peak, half-peak width, and charge transfer values found here and by *Jerauld* [2007] are consistent with estimates of leader-step current waveform parameters (based on distant electric field measurements) reported by *Krider et al.* [1977] for stepped leaders. However, it has been shown that the current model of the leader step must include a slow front to replicate intrinsic features observed in the dE/dt leader-step waveforms. *Krider et al.* [1977] suggested that the peak step current is at least 2–8 kA and that the minimum charge transfer of a step is 1–4 mC. *Rakov* [1998] gave similar estimates for dart-stepped leaders. However, the peak dI/dt value found here of approximately 100 kA μs^{-1}, and similarly by *Jerauld* [2007], is much larger than the 6–24 kA μs^{-1} reported by *Krider et al.* [1977] and is similar to that observed for return strokes [e.g., *Krider et al.*, 1996].

21562202d, 2011, D8, Downloaded from https://agupubs.onlinelibrary.wiley.com/doi/10.1029/2010JD015249, Wiley Online Library on [28/07/2025]. See the Terms and Conditions (https://onlinelibrary.wiley.com/terms-and-conditions) on Wiley Online Library for rules of use; OA articles are governed by the applicable Creative Commons License

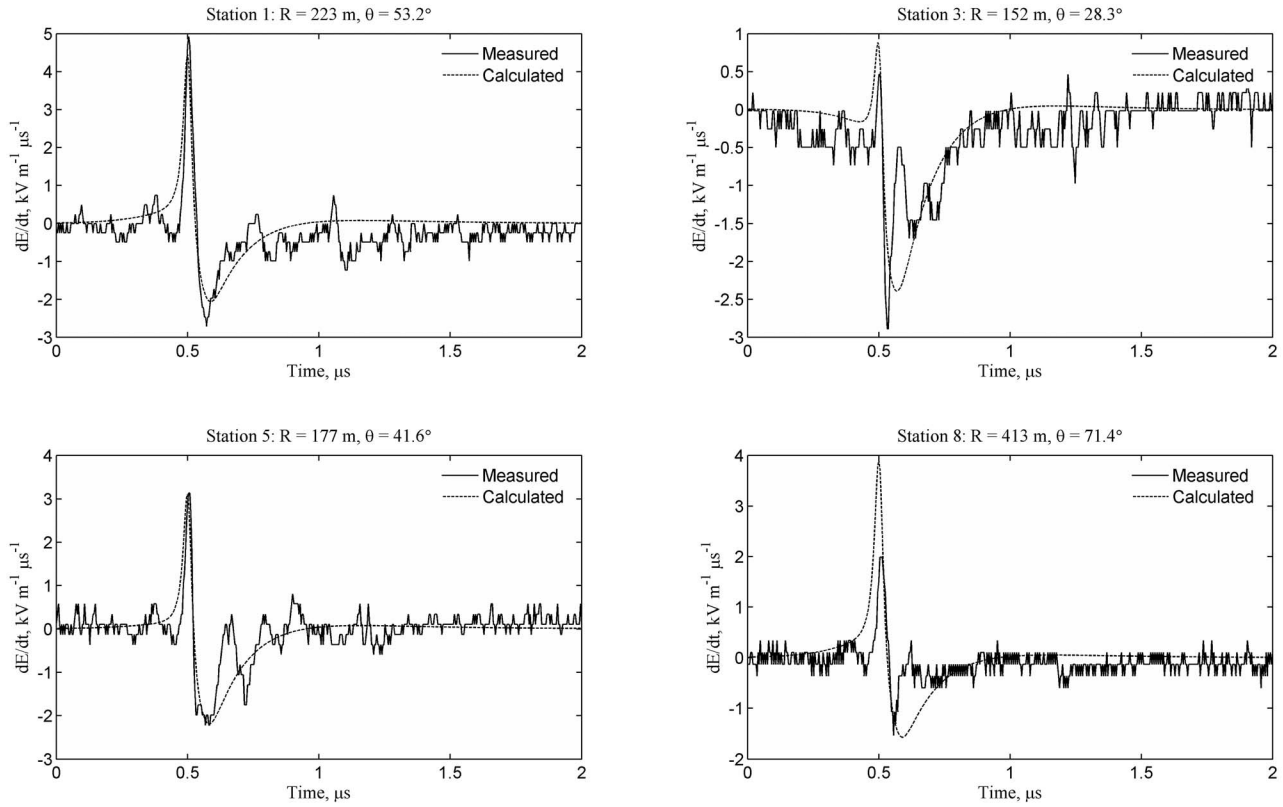

Figure 16. Step A modeling from lightning event MSE0604. The current front propagated with an upward speed of 1.5×10^8 m s^{-1}, and the amplitude of the current waveform decayed exponentially with a decay constant of 25 m. Note that the waveform at Station 3 decreases prior to the main peak while the waveform of the other three stations is flat or increases. The slow front on the current in Figure 15 is needed to reproduce these effects.

21562202d, 2011, D8, Downloaded from https://agupubs.onlinelibrary.wiley.com/doi/10.1029/2010JD015249, Wiley Online Library on [28/07/2025]. See the Terms and Conditions (https://onlinelibrary.wiley.com/terms-and-conditions) on Wiley Online Library for rules of use; OA articles are governed by the applicable Creative Commons License

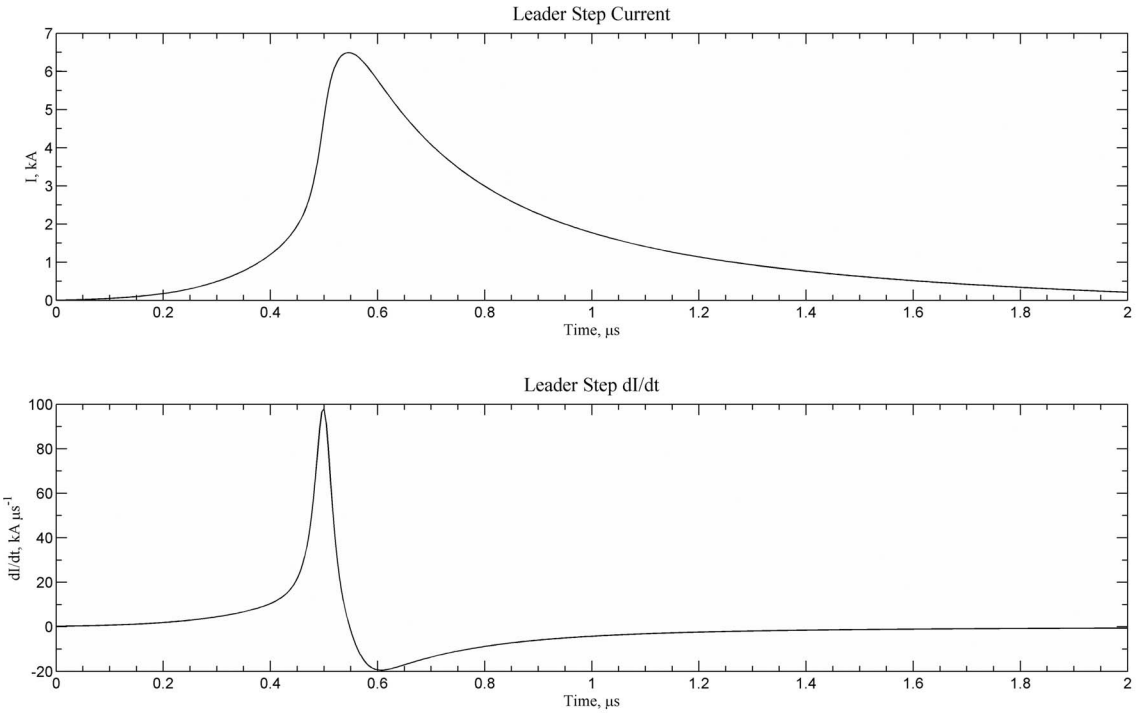

Figure 17. Current and current derivative waveforms used in modeling Step B. The current derivative waveform was generated using equation (7) with the parameters T_{peak} = 0.5 μs, α_1 = 118 kA μs^{-1}, α_2 = 10.5 kA μs^{-1}, β = 1.85, and γ = 20 ns.

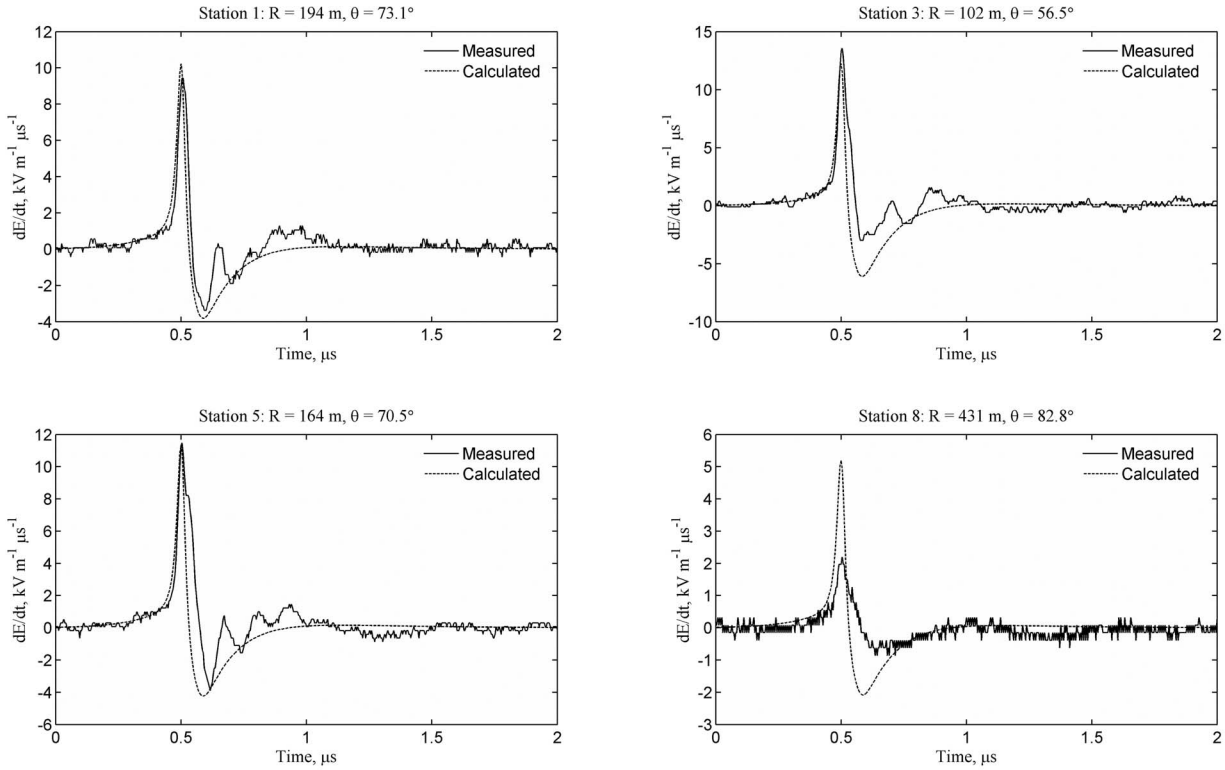

Figure 18. Step B modeling from lightning event MSE0604. The current front propagated with an upward speed of 1.5×10^8 m s^{-1}, and the amplitude of the current waveform decayed exponentially with a decay constant of 25 m.

21562202d, 2011, D8, Downloaded from https://agupubs.onlinelibrary.wiley.com/doi/10.1029/2010JD015249, Wiley Online Library on [28/07/2025]. See the Terms and Conditions (https://onlinelibrary.wiley.com/terms-and-conditions) on Wiley Online Library for rules of use; OA articles are governed by the applicable Creative Commons License

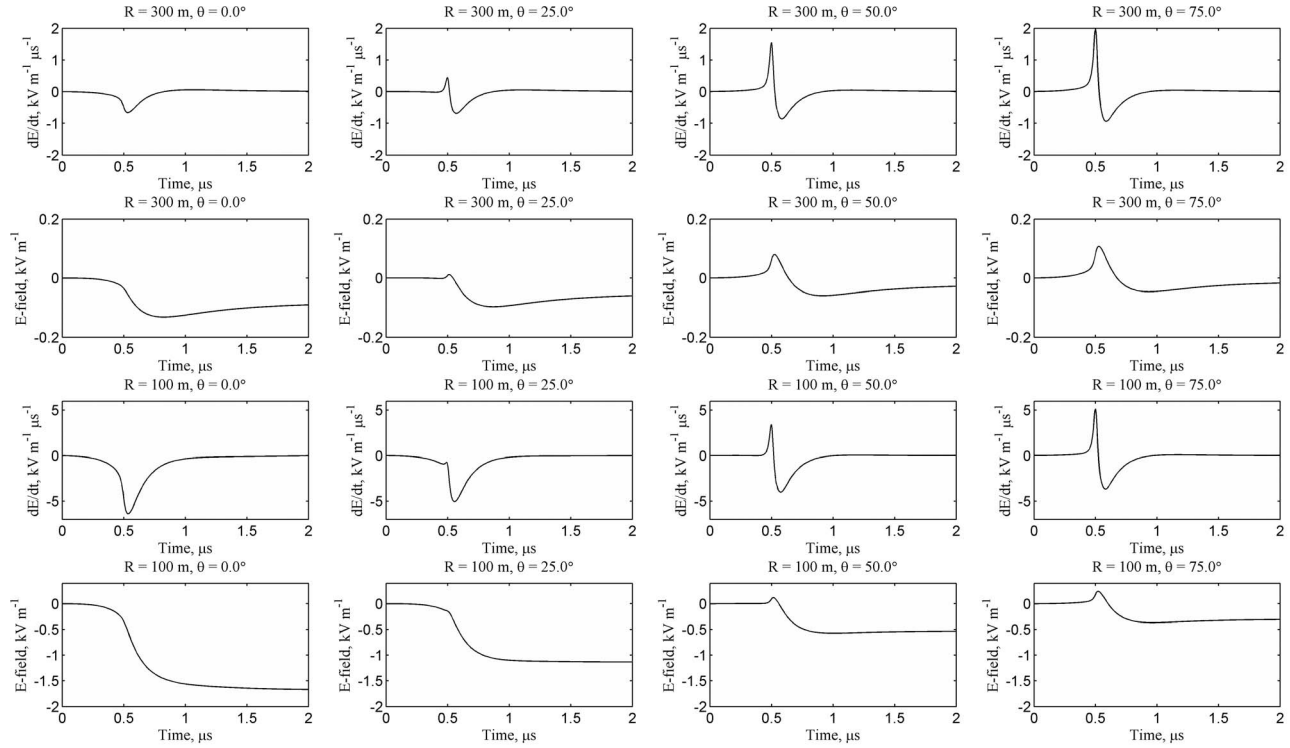

Figure 19. Illustrations of leader-step electric field derivative (dE/dt) and electric field (E-field) variation with respect to range (R) and angle (θ), as shown in Figure 4. The first and second rows show leader-step dE/dt and E-field waveforms, respectively, for various angles at a range of 300 m. The third and fourth rows show waveforms for various angles at a range of 100 m. The vertical scales for the 100 m and 300 m calculations are different. All waveforms are modeled using the current (I) and current derivative (dI/dt) parameters specified in Figure 17.

[24] Finally, using the current and current derivative waveforms of Figure 17, we compute and show in Figure 19 the predicted dE/dt and E-field leader-step waveforms at a variety of ranges and angles. These model fields exhibit the leader-step waveform characteristics discussed above: a dominant initial peak that is reduced as the step channel is seen end-on and an opposite polarity overshoot that increases relative to the initial peak with decreasing range.

6. Summary and Conclusion

[25] This paper has examined the characteristics of stepped-leader dE/dt pulses at close range. From an examination of the waveforms, the characteristic shape of a close leader-step dE/dt pulses can be described as a bipolar pulse having a sharp initial half cycle with the same polarity as the return-stroke pulse, followed by an opposite polarity overshoot which decays relatively slowly to the background level. The initial peak is often preceded by a slow front, similar to the slow front that precedes the fast transition to peak in first return stroke dE/dt and E waveforms. The observed and modeled waveforms indicate that the initial peak of the dE/dt leader-step waveform is dependent on the horizontal distance, angle (θ) between the line of sight and vertical, and channel orientation. Conversely, the amplitude of the opposite polarity overshoot appears to be dominated by its dependence on distance, with the overshoot typically being largest in the closest waveforms and barely noticeable in the farthest. The effect of the angle (θ) between the line of sight and vertical on the initial peak amplitude can be observed in many steps, for example, in Figures 6 and 7, where the closest waveform exhibits a smaller initial peak than farther waveforms, due to the small angle (θ) associated with the closest station. Indeed, an examination of Figure 19, in which all parameters (e.g., current amplitude and waveshape, wavefront velocity, current decay with height) were held constant except for $|\boldsymbol{R}|$ and θ, clearly indicates that the initial peak decreases as θ approaches zero. The effect of the leader channel orientation has been observed in the data, but no example is given in which the Station 3 and Station 5 waveforms exhibited significantly different initial peaks despite the ranges and angles between the line of sight and vertical for these two measurements being nearly identical. Although the unknown orientation of the actual leader channel clearly affects the observed dE/dt pulses, our leader-step modeling always assumed a straight and vertical leader channel.

[26] The dE/dt leader steps occurring within 100 μs of the first stroke of flashes MSE0604, MSE0703, and MSE0704 were analyzed for half-peak width, 10–90% risetime, and the peak value range-normalized to 100 km. Over the distance range examined, no distance dependence was detected. The mean value of the half-peak width was found to be 33.5 ns, with a standard deviation of 11.9 ns. This value is nearly half the value previously reported by *Willett and Krider* [2000] for the half-peak width (54 ns with a standard deviation of 17 ns)

21562202d, 2011, D8, Downloaded from https://agupubs.onlinelibrary.wiley.com/doi/10.1029/2010JD015249, Wiley Online Library on [28/07/2025]. See the Terms and Conditions (https://onlinelibrary.wiley.com/terms-and-conditions) on Wiley Online Library for rules of use; OA articles are governed by the applicable Creative Commons License

under conditions in which propagation effects were expected to be small. The mean peak of the dE/dt step pulses, range-normalized to 100 km, was found to be 7.4 V m^{-1} μs^{-1} (standard deviation of 3.7 V m^{-1} μs^{-1}). However, we have discussed why these values may underestimate the actual value by as much as a factor of 1.2 to 2. Interestingly, *Krider et al.* [1992] reported the mean peak dE/dt step pulses, range-normalized to 100 km, to be 13 V m^{-1} μs^{-1}. Finally, we determined the 10–90% risetime to be 43.6 ns (standard deviation of 24.2 ns).

[27] Two stepped-leader pulses that were relatively free of secondary pulses were identified for leader modeling. A current function introduced by *Jerauld* [2007], originally for estimating the current derivative of first return strokes, was found to provide adequate modeling of the measured leader-step fields. The current waveforms obtained from the model had half-peak widths of about 300 ns and maximum rates of current rise of about 100 kA μs^{-1}. The charge transfer and peak current predicted from the model were ~3 mC and 5–7 kA, respectively. An important physical result of the modeling is that the step-leader current often must contain a slow front, similar to that observed in natural first strokes, in order to reproduce the observed dE/dt leader-step waveforms.

[28] **Acknowledgments.** This research was funded in part by DARPA grants HR0011-08-1-0088 and HR0011-1-10-1-0061 and by NSF grant ATM 0852869.

References

Beasley, W. H., M. A. Uman, D. M. Jordan, and C. Ganesh (1983), Simultaneous pulses in light and electric field from stepped leaders near ground level, *J. Geophys. Res.*, *88*, 8617–8619, doi:10.1029/JC088iC13p08617.

Cooray, V. (1987), Effects of propagation on the return stroke radiation fields, *Radio Sci.*, *22*, 757–768, doi:10.1029/RS022i005p00757.

Cooray, V. (2009), Propagation effects due to finitely conducting ground on lightning-generated magnetic fields evaluated using Sommerfeld's integrals, *IEEE Trans. Electromagn. Compat.*, *51*(3), doi:10.1109/TEMC.2009.2019759.

Cooray, V., M. Fernando, T. Sörensen, T. Götschl, and A. Pedersen (2000), Propagation of lightning generated transient electromagnetic fields over finitely conducting ground, *J. Atmos. Terr. Phys.*, *62*, 583–600, doi:10.1016/S1364-6826(00)00008-0.

Heidler, F. (1985), Traveling current source model for LEMP calculation, paper presented at 6th International Symposium on Electromagnetic Compatability, St. Petersburg Electrotech. Univ., St. Petersburg, Russia.

Howard, J., M. A. Uman, C. Biagi, D. Hill, J. Jerauld, V. A. Rakov, J. Dwyer, Z. Saleh, and H. Rassoul (2010), RF and X-ray source locations during the lightning attachment process, *J. Geophys. Res.*, *115*, D06204, doi:10.1029/2009JD012055.

Jerauld, J. (2007) Properties of natural cloud-to-ground lightning inferred from multiple-station measurements of close electric and magnetic fields and field derivatives, Ph.D. dissertation, Univ. of Fla., Gainesville. (Available at http.//purl.fcla.edu/fcla/etd/UFE0021279)

Jerauld, J., M. A. Uman, V. A. Rakov, K. J. Rambo, D. M. Jordan, and G. H. Schnetzer (2008), Electric and magnetic fields and field derivatives from lightning stepped leaders and first return strokes measured at distances from 100 to 1000 m, *J. Geophys. Res.*, *113*, D17111, doi:10.1029/2008JD010171.

Koshak, W. J., et al. (2004), North Alabama Lightning Mapping Array (LMA): VHF source retrieval algorithm and error analysis, *J. Atmos. Oceanic Technol.*, *21*, 543–558, doi:10.1175/1520-0426(2004)021<0543:NALMAL>2.0.CO;2.

Krider, E. P., and G. J. Radda (1975), Radiation field wave forms produced by lightning stepped leaders, *J. Geophys. Res.*, *80*, 2653–2657, doi:10.1029/JC080i018p02653.

Krider, E. P., C. D. Weidman, and R. C. Noggle (1977), The electric field produced by lightning stepped leaders, *J. Geophys. Res.*, *82*, 951–960, doi:10.1029/JC082i006p00951.

Krider, E. P., C. Leteinturier, and J. C. Willett (1992), Submicrosecond field variations in natural lightning processes, *Res. Lett. Atmos. Electr.*, *12*, 3–9.

Krider, E. P., C. Leteinturier, and J. C. Willett (1996), Submicrosecond fields radiated during the onset of first return strokes in cloud-to-ground lightning, *J. Geophys. Res.*, *101*, 1589–1597, doi:10.1029/95JD02998.

Murray, N. D., E. P. Krider, and J. C. Willett (2005), Multiple pulses in dE/dt and the fine-structure of E during the onset of first return strokes in cloud-to-ocean lightning, *Atmos. Res.*, *76*, 455–480, doi:10.1016/j.atmosres.2004.11.038.

Norton, K. A. (1937), Propagation of radio waves over the surface of the Earth and in the upper atmosphere, II, *Proc. IEEE*, *25*, 1203–1236.

Nucci, C. A., C. Mazzetti, F. Rachidi, and M. Ianoz (1988), On lightning return stroke models for LEMP calculations, paper presented at 19th International Conference on Lightning Protection, ICLP Cent., Graz, Austria.

Rakov, V. A. (1998), Some inferences on the propagation mechanisms of dart leaders and return strokes, *J. Geophys. Res.*, *103*, 1879–1887, doi:10.1029/97JD03116.

Rakov, V. A., and A. A. Dulzon (1987), Calculated electromagnetic fields of lightning return stroke, *Tekh. Elektrodinam.*, *1*, 87–89.

Rakov, V. A., and M. A. Uman (1998), Review and evaluation of lightning return stroke models including some aspects of their application, *IEEE Trans. Electromagn. Compat.*, *40*(4), 403–426, doi:10.1109/15.736202.

Schoene, J., M. A. Uman, V. A. Rakov, K. J. Rambo, J. Jerauld, and G. H. Schnetzer (2003), Test of the transmission line model and traveling current source model with triggered lightning return strokes at very close range, *J. Geophys. Res.*, *108*(D23), 4737, doi:10.1029/2003JD003683.

Thomas, R. J., P. R. Krehbiel, W. Rison, S. J. Hunyady, W. P. Winn, T. Hamlin, and J. Harlin (2004), Accuracy of the Lightning Mapping Array, *J. Geophys. Res.*, *109*, D14207, doi:10.1029/2004JD004549.

Thottappillil, R., V. A. Rakov, and M. A. Uman (1997), Distribution of charge along the lightning channel: Relation to remote electric and magnetic fields and to return-stroke models, *J. Geophys. Res.*, *102*(D6), 6987–7006, doi:10.1029/96JD03344.

Uman, M. A., and D. K. McLain (1969), Magnetic field of the lightning return stroke, *J. Geophys. Res.*, *74*, 6899–6910, doi:10.1029/JC074i028p06899.

Uman, M. A., D. K. McLain, and E. P. Krider (1975), The electromagnetic radiation from a finite antenna, *Am. J. Phys.*, *43*, 33–38, doi:10.1119/1.10027.

Uman, M. A., C. E. Swanberg, J. A. Tiller, Y. T. Lin, and E. P. Krider (1976), Effects of 200 km propagation on lightning return stroke electric fields, *Radio Sci.*, *11*, 985–990, doi:10.1029/RS011i012p00985.

Weidman, C. D., and E. P. Krider (1980), Submicrosecond risetimes in lightning radiation fields, *NASA Conf. Publ.*, *2128*, 29–38.

Willett, J. C., and E. P. Krider (2000), Rise times of impulsive high-current processes in cloud-to-ground lightning, *IEEE Trans. Antennas Propag.*, *48*(9), 1442–1451, doi:10.1109/8.898779.

Willett, J. C., V. P. Idone, R. E. Orville, C. Leteinturier, A. Eybert-Berard, L. Barret, and E. P. Krider (1988), An experimental test of the "transmission-line model" of electromagnetic radiation from triggered lightning return strokes, *J. Geophys. Res.*, *93*, 3867–3878, doi:10.1029/JD093iD04p03867.

C. Biagi, D. Hill, D. M. Jordan, V. A. Rakov, and M. A. Uman, Department of Electrical and Computer Engineering, University of Florida, Gainesville, FL 32611, USA.

J. Howard, Sandia National Laboratories,MS 0878, Albuquerque, NM 87185-0878, USA. (ironjoe@ufl.edu)

215622024, 2011, D8, Downloaded from https://agupubs.onlinelibrary.wiley.com/doi/10.1029/2010JD015249, Wiley Online Library on [28/07/2025]. See the Terms and Conditions (https://onlinelibrary.wiley.com/terms-and-conditions) on Wiley Online Library for rules of use; OA articles are governed by the applicable Creative Commons License